MODEL Z BY COMPUTATION AND TAYLOR'S CONDITION

D. JAULT

*Department of Mathematics and Statistics, The University,
Newcastle Upon Tyne, NE1 7RU, UK**

The spherical geodynamo model of Braginsky (1978) is re-integrated. The original model of Braginsky modified the Taylor's condition to include the influence of viscous core-mantle coupling. Reinstating also the ϕ-component of momentum $\partial \omega_G(s)/\partial t$ [where $\omega_G(s)$ is the geostrophic shear] in the expression for the modified Taylor condition makes possible the investigation of solutions for small viscosities. Above a critical dynamo number D_c, the solution enters a viscously-limited branch ("Ekman" or "coupling" branch) and, eventually, as D is further increased, jumps to a strong-field branch. The original numerical solution of Braginsky belongs to the latter branch and is duplicated. But, with weak viscosities, the solution on that branch is proved inviscid. In that inviscid limit, Braginsky's model meets the Taylor's condition. The same code is used to re-investigate another $\alpha\omega$ dynamo model defined by a simpler choice of α and ω effects $[\alpha = R_x \cos\theta, \omega = R_\omega(r-1)]$.

KEY WORDS: $\alpha\omega$ dynamos, Taylor's condition, model Z, earth's core.

1. INTRODUCTION

It is generally believed that a balance is struck, inside the Earth's outer fluid core, between magnetic and Coriolis forces. "Intermediate" dynamo models have been devised to study this balance. In these models, the distribution of density heterogeneities, which provide the energy source, is prescribed. The momentum equation, where the acceleration $\partial v/\partial t$ and the viscous forces are neglected, is diagnostic and allows us to derive the velocity v from the magnetic field. But, that solution is not unique (arbitrary geostrophic motions can be added) and can be found if and only if the action of the magnetic forces on the geostrophic cylinders vanishes (Taylor, 1963). Different studies have shown how imposing the Taylor's condition determines the geostrophic velocity, up to a bulk rotation of the core (Taylor, 1963; Fearn and Proctor, 1987). The very existence of "Taylor states" (magnetic field solutions obeying the Taylor's condition) has been subjected to many investigations. Most of them have approached the Taylor's condition by taking into account small mass flux in the Ekman boundary layers below the core surface (Tough and Roberts, 1968). This makes the mathematical problem well posed: from a given magnetic field, an unique velocity field can always be found and can then be used to time-step the induction equation. It is

---

* Permanent address: Laboratoire de Géomagnétisme, URA 729 du CNRS, Institut de Physique du Globe de Paris, 4 place Jussieu, 75252 PARIS CEDEX 05, FRANCE

then possible to test whether the solution opts for a Taylor state in the limit of vanishing viscosity.

Investigations of that question have relied on numerical integrations of nearly axisymmetrical dynamo models (Barenghi and Jones, 1991; Hollerbach and Ierley, 1991; Barenghi, 1992; Hollerbach et al., 1992; Barenghi, 1993). A prescribed α effect models generation of the mean axisymmetrical field by planetary waves (Braginsky, 1964). Shearing the meridional field by the azimutal thermal wind ω_T is called the ω effect.

The dynamo number D measures the product of the amplitude of the α and ω effects. These studies have found that above a critical dynamo number D_c, the solution enters a coupling (or Ekman) regime where it scales as $\varepsilon^{1/2}$ ($\varepsilon = E^{1/2}$ and E is the Ekman number). In some cases ($\alpha^2, \alpha^2\omega$ models), large dynamo number solutions have been proved inviscid. Then, this sequence of regimes is said to follow the Malkus-Proctor scenario after the authors of the 1975 paper where it was first sketched.

Braginsky (1975) suggested another view of the asymptotics ($\varepsilon \to 0$). He envisioned that the action of the magnetic forces on the geostrophic cylinders, which depends on

$$\frac{d}{ds}\left(s^2 \int BB_s\, dz \right)$$

where s is the cylindrical radius, B is the ϕ-component of the magnetic field, is made small because the meridional field lines are increasingly parallel to the rotation axis Oz [$B_s = O(\varepsilon^{1/3})$]. As ε is decreased, the action of the magnetic forces on the geostrophic cylinders, though small, does not vanish; it is balanced by the mass flux in the Ekman boundary layers, which continues to play an important part because the geostrophic velocity (the dominant part of the fluid velocity at the core surface) increases as $\varepsilon^{-2/3}$. Thus the solution he envisaged never attains an inviscid limit. We shall not detail any further the model-Z theory, of which the main ingredient is a boundary layer analysis. Let us only note that it is a non-linear theory. Braginsky (1978) and Braginsky and Roberts (1987) presented numerical integrations of a particular $\alpha\omega$ dynamo, with an intricate geometry of the α effect, to support that theoretical analysis. They were not able to study the limit ($\varepsilon \to 0$) and did not prove the asymptotic form proposed by Braginsky (1975) but the model Z character of their solution was clear: most of the lines of force of the meridional field are parallel to the symmetry axis. Furthermore, Braginsky's dynamo model is steady-state in contrast to the other $\alpha\omega$ dynamo models reported in the literature. In this paper, it is shown that both the geometry and the steadiness of the numerical model Z can be accounted for by the geometry of the prescribed α effect: the kinematic solution, at the onset of dynamo action, shows Z geometry. The limit ($\varepsilon \to 0$) is studied and the Malkus-Proctor scenario is shown to apply.

Section 2 and 3 present, respectively, the basic equations and the numerical method used. Section 4 investigates the solution for a reference $\alpha\omega$ model $\alpha = \alpha_0 \cos\theta$, $\omega = \omega_0(r - 1)$, discussing the approach to the Taylor's regime. Section 5 deals with Braginsky's numerical model. The final section gives scope for further work, comparing different equations governing the geostrophic velocity. Geophysical implications of the study are outlined also.

2. BASIC EQUATIONS

Description of $\alpha\omega$ axisymmetrical dynamos equations can be found elsewhere (eg. Fearn et al., 1988, pp 179–201, 289–305) and is not recalled here. Following Braginsky (1978) and Braginsky and Roberts (1987), the axisymmetrical parts of the magnetic field and of the fluid velocity are written:

$$\mathbf{B} = B\mathbf{e}_\phi + \mathbf{V} \times \left(\frac{\psi}{s}\mathbf{e}_\phi\right) = \mathbf{B}_T + \mathbf{B}_P,$$

$$\mathbf{v} = s[\omega_T + \omega_B + \omega_G(s)]\mathbf{e}_\phi + \mathbf{V} \times \left(\frac{\chi}{s}\mathbf{e}_\phi\right) = \mathbf{v}_T + \mathbf{v}_P,$$

where ω_T is the prescribed thermal wind, ω_B is the magnetic wind created by magnetic forces and ω_G is the geostrophic shear.

The Coriolis force is large compared with the inertial forces which are, except for $\partial\omega_G/\partial t$, neglected in the momentum equation. Thus ω_B and χ are determined from the magnetic field components B and ψ. Time-stepping of the induction equation determines both B and ψ (see again Braginsky and Roberts, 1987). With scaled variables:

$$\frac{\partial B}{\partial t} = -D(B) + \Delta B + sB_s\frac{d\omega_G}{ds} + R_\omega s\mathbf{B}_p\cdot\mathbf{V}\omega_T, \tag{1}$$

$$\frac{\partial\psi}{\partial t} = -\mathbf{V}\cdot(\psi\mathbf{v}_p) + \Delta^-\psi + R_\alpha s\alpha B \tag{2}$$

with

$$\Delta B = \left(\nabla^2 - \frac{1}{s^2}\right)B, \quad \Delta^-\psi = \frac{\partial^2\psi}{\partial r^2} + \frac{\sin\theta}{r^2}\frac{\partial}{\partial\theta}\left(\frac{1}{\sin\theta}\frac{\partial\psi}{\partial\theta}\right),$$

$$D(B) = \mathbf{V}\cdot(B\mathbf{v}_p) + \frac{1}{s^2}B_sB^2 - \frac{3}{s}B\mathbf{B}_p\cdot\mathbf{V}B,$$

$(2\Omega\mu\rho\eta)^{1/2}$ is unit of magnetic field, $\eta = 1/\mu\sigma$ is magnetic diffusivity, σ is conductivity, μ is permeability, Ω is Earth's rotation rate, the core radius a is unit of length, a^2/η is unit of time. The Reynolds numbers R_α and R_ω measure respectively the size of the α and ω effects. The poloidal velocity $\mathbf{v}_p$ is calculated from its s-component v_s, derived from the ϕ-component of the momentum equation

$$v_s = \frac{1}{s}\mathbf{B}_p\cdot\mathbf{V}(sB). \tag{3}$$

Braginsky (1975) assumed the zonal terms to be large compared to the meridional ones. Therefore, the part of the magnetic wind ω_B depending on B_p^2 can be neglected and the α-effect term can be omitted in the toroidal equation. Also, the balance between the viscous core-mantle friction at the CMB and the action of the magnetic forces on the geostrophic cylinders inside the core then reduces to

$$\omega_G = \frac{z_1^{1/2}}{2\rho E^{1/2}\Omega a\mu s^3}\frac{d}{ds}\left(s^2\int_{-z_1}^{z_1} B_s B\,dz\right) \tag{4}$$

where $z_1^2 + s^2 = a^2$, Ω is Earth's rotation rate, ν is viscosity, $E = \nu/\Omega a^2$ is Ekman number. However, Fearn et al. (1988) stressed that it is not legitimate, in the framework of the model-Z theory, to neglect the momentum term $\partial\omega_G/\partial t$ since oscillations around the equilibrium are damped on a spin-up time scale $(E^{1/2}\Omega)^{-1}$ which is not small. When the $\partial\omega_G/\partial t$ term is retained, (4) has to be replaced by

$$\frac{\partial\omega_G}{\partial t} + \frac{E^{1/2}\Omega}{z_1^{3/2}}\omega_G - \frac{1}{2\rho\mu s^3 a z_1}\frac{d}{ds}\left(s^2\int_{-z_1}^{z_1} BB_s\,dz\right) = 0. \tag{5}$$

With scaled variables, (4) and (5) are respectively transformed into

$$\omega_G = \frac{z_1^{1/2}\varepsilon^{-1}}{s^3}\frac{d}{ds}\left(s^2\int_{-z_1}^{z_1} B_s B\,dz\right), \tag{6}$$

$$Ro\frac{\partial\omega_G}{\partial t} + \frac{\varepsilon\omega_G}{z_1^{3/2}} - \frac{1}{s^3 z_1}\frac{d}{ds}\left(s^2\int_{-z_1}^{z_1} BB_s\,dz\right) = 0, \tag{7}$$

with $\varepsilon = E^{1/2}$, $Ro = \eta/\Omega a^2$ is Rossby number. The parameters Ro and ε allow us to compare the timescales entering the problem with the ohmic decay time a^2/η: $2\pi Ro$ measures the rotation period and Ro/ε the Ekman spin-up timescale. We have time-stepped either (1) or (2) [with expression (6) substitued for ω_G in (1)] or (1),(2),(7). When (7) is used the ϕ-component of the momentum equation yields instead of (3)

$$v_s = \frac{1}{s}\mathbf{B}_p\cdot\nabla(sB) - \frac{sRo}{2}\frac{\partial\omega_G}{\partial t}, \tag{8}$$

and, as a consequence,

$$D(B) = \nabla\cdot(\mathbf{B}v_p) + \frac{1}{s^2}B_s B^2 - \frac{3}{s}B\mathbf{B}_p\cdot\nabla B + \frac{Ro}{2}B\frac{\partial\omega_G}{\partial t}.$$

Taylor (1963) suggested another method to calculate the geostrophic velocity, which is straightforward when applied to axisymmetrical solutions. Here, the Taylor's

condition [(7) with $\varepsilon = Ro = 0$] is

$$\forall s_0 \qquad \frac{d}{ds}\left(s^2 \int_{s=s_0} BB_s dz \right) = 0. \tag{9}$$

Discarding magnetic field solutions singular at the axis, we get

$$\forall s_0 \qquad \int_{s=s_0} BB_s dz = 0. \tag{10}$$

Then, following Taylor (1963), we take the time derivative of the identity (10) and we replace the terms $\partial B/\partial t$ and $\partial B_s/\partial t$ by their expression inferred from (1) and (2). This yields a relation involving the geostrophic shear ω_G. Braginsky (1975) showed how to arrange the different terms to get:

$$\left(\int_{-z_1}^{z_1} sB_s^2 dz \right)\frac{d\omega_G}{ds} = -\int_{-z_1}^{z_1} sB_s\mathbf{B}_p\cdot\nabla\omega_T dz + s^2\int_{-z_1}^{z_1}\left(\mathbf{B}_p\cdot\nabla\left(\frac{B}{s}\right)\right)^2 dz$$

$$-\int_{-z_1}^{z_1}\left(B_s\Delta B + B\Delta B_s + \alpha B\frac{\partial B}{\partial z} \right)dz. \tag{11}$$

The Taylor solution (11) for $sd\omega_G/ds$ can be compared with the same quantity obtained along with the magnetic field solution. We shall see (Section 4) that it may shed light on the approach to the Taylor regime by the solution for the Steenbeck and Krause model. On the other hand, such a comparison gives no indication on the solutions for the Braginsky's model because steady solutions always satisfy (11). Incidentally, (11) is first-order in contrast with the more general second-order equation of Taylor (1963) [his equation (4.5)] because we have already discarded a solution (singular at the origin) whilst writing (10). An inspection of (11) shows that the Taylor solution for $sd\omega_G/ds$ may be O(1) at the axis (then $\omega_G\to\infty$ logarithmically as $s\to 0$) (see also Section 6).

3. NUMERICAL METHOD

The method used is very similar to the method set out by Braginsky and Roberts (1987). Few improvements have been implemented and the reader is referred to Braginsky (1978) and Braginsky and Roberts (1987). Only solutions with dipole symmetry are reported here. Finite differences in both directions are used. Most of the calculations are done with a spherical grid. ($0 < r \leqslant 1$, $0 < \theta \leqslant \pi/2$) but a cylindrical grid is necessary to evaluate the meridional and the geostrophic velocity. Linear interpolations are performed between the cylindrical and the spherical grids. The density of points increases as $r \to 1$ in order to study the magnetic boundary layer. As a consequence, the spacings are not uniform and some of the numerical schemes are not second-order accurate. There are NR points in r and NL in θ. Different truncation

levels ($33 < NR \leqslant 120$, $33 \leqslant NL \leqslant 180$) have been used. The cylindrical grid is slightly different from the grid used by Braginsky and Roberts. It has been built in such a way as to make the local density of points for the two grids similar everywhere. In particular, it is not equally spaced in s in order again to sample the magnetic boundary-layer. Following Braginsky (1978), decomposition in spherical harmonics is used to implement the matching conditions for the poloidal field B_p at the boundary with the insulating container. Numerical convergence with respect to the size $NLEG$ of the set of Legendre polynomials entering the decomposition is monitored. Also, because electrical currents flowing in the Ekman boundary layer make the horizontal component of $\mathbf{B}_p$ discontinuous through that layer, a jump in ψ, at the core surface, is calculated [see again Braginsky and Roberts (1987)]. Diffusion in r and θ is treated with the Alternative Direction Implicit (ADI) method. Most of the other terms are treated with the explicit Adams-Bashforth method. The poloidal equation is integrated first. As a consequence, the Crank-Nicholson method can be used to compute the thermal wind in the toroidal equation. The s-derivative of the geostrophic shear is calculated at semi-intervals of the cylindrical grid. Otherwise, namely if $sd\omega_G/ds$ was computed in the obvious way, i.e. on the same cylindrical grid (s_i) [i] as ω_G, before being interpolated on the spherical grid, $[\omega_G(s_{i+1}) - \omega_G(s_{i-1})]$ alone would play a part in the induction equation, the solutions for $\omega_G(s_{2i})$ and $\omega_G(s_{2i+1})$ would be decoupled, and, with small viscosities, on the strong-field branch, serrated geostrophic profiles would be obtained.

Braginsky (1975) introduced a dimensionless parameter R, which he called the magnetic Reynolds number

$$R = \frac{av_T}{\eta}.$$

Then, he showed that the equations (1), (2), (5), (7) are not changed when the variables are scaled as

$$B = R^{1/2}B', \quad \psi = R^{-1/2}\psi'$$

$$\varepsilon = \frac{\varepsilon'}{R}, \quad Ro = \frac{Ro'}{R}, \quad R_\omega = RR'_\omega, \quad R_\alpha = \frac{R'_\alpha}{R}$$

Those transformations (with $R = R_\omega$) make clear that two ($D = R_\alpha R_\omega$, $\varepsilon' = R_\omega \varepsilon$) or three ($D$, ε', $Ro' = R_\omega Ro$) parameters only are independent. In order to compare our results with both Braginsky (1978) and Braginsky and Roberts (1987), we have retained the set of parameters (R_α, R_ω, ε) that they used [plus Ro when (7) and (8) are used]. So there is a redundant parameter, and the parameter space can be entirely scanned with the ratio R_ω/R_α kept fixed. We have imposed $|R_\omega/R_\alpha| = 10$ and ε and Ro can be set to model accurately the Earth's fluid core. Both depend on R. Braginsky (1975) noted that, with $R = 100$, the actual intensity of the Earth's dipolar field, as well as the size of the velocity field calculated from Earth's magnetic field secular variation data, both at the core surface, are modelled by quantities with values close to 1. Viscosity of the fluid in the Earth's core is very small, on the order of 3×10^{-2} P. (Poirier, 1988). It gives

$E = 1.5 \times 10^{-13}$ and with $R = 100$, $\varepsilon = 4 \times 10^{-5}$. The Rossby number Ro is 7×10^{-7} again with $R = 100$.

4. STEENBECK AND KRAUSE CHOICE OF α AND ω EFFECTS

We shall refer to

$$\alpha(r, \theta) = R_\alpha \cos \theta, \quad \omega_T(r, \theta) = R_\omega(r - 1)$$

as the Steenbeck and Krause choice. It defines a geodynamo model which is now a benchmark. It has been studied at depth by Roberts (1972), Barenghi and Jones (1991) and Hollerbach *et al.* (1992). We shall report here results for $D = R_\alpha R_\omega < 0$. The conclusions drawn from the studies of the $D < 0$ and $D > 0$ cases are broadly similar. In that part, the $\partial \omega_G / \partial t$ term shall be neglected and (6) shall be used.

Testing the programe with that model was deemed necessary. Both Braginsky (1978) and Roberts (1989) reported that, using codes similar to ours, they could not get solutions with a smooth α. Braginsky (1978) noted that he did not get solutions for the simplest choices of α effect because the seed field was expelled from the regions where α is large whereas Roberts (1989) observed that large gradients in the geostrophic velocity developed until numerical instability occurred. Barenghi and Jones (1991) wondered whether these failures can be accounted for by difficulties encountered in the calculation of the geostrophic velocity. They devised a code which ensures that the geostrophic shear term, in the induction equation, does not feed energy in the magnetic field. Indeed, studying the changes in the toroidal magnetic energy, Braginsky (1975) had shown that the only energy source originates from the thermal wind. Magnetic induction due to the geostrophic velocity is the counterpart of the work done by magnetic forces against viscous friction (here, changes in the kinetic energy associated with the term $\partial \omega_G / \partial t$ are neglected). We have taken this remark into account and we have checked, at each time step, that the contribution of the geostrophic term to the magnetic energy budget remains negative. Let us now summarize the results.

At the onset of dynamo action, the solution is oscillatory. The critical dynamo number is $D_c = -5526$ and the oscillation frequency is $\omega_c = 54.18$ (with $NR = NL = 60$) in agreement with both Roberts (1972) and Barenghi and Jones (1991). As the dynamo number D is increased above its critical value, the solution enters a viscously limited regime, which has been described by Barenghi and Jones (1991) and Hollerbach *et al.* (1992). It consists of dynamo waves which scale as $\varepsilon^{1/2}$. This geometry compares well with previous results. However, we do not confirm that the Ekman branch solution loses stability as D is further increased. At $D \approx -35000$, the solution becomes doubly periodic. It is reminiscent of the bifurcation reported by Barenghi and Jones (1991). However, in contrast with their results, it turns out that beyond $D \approx -35000$, the geostrophic term alone is still capable of equilibrating the field. Figure (1) shows that the amplitude of the solution increases dramatically around $D \approx -35000$ but it does not diverge to infinity as D rises further. Now, we argue that this viscously-limited branch is strongly influenced by the Taylor's condition.
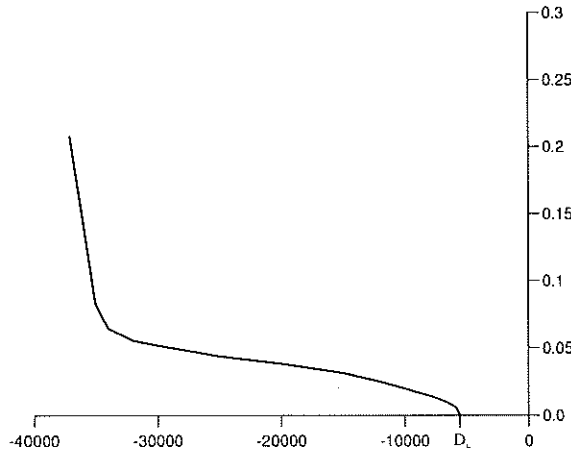
Figure 1 $(\langle (B_p^{\mathrm{max}})^2 \rangle^{1/2} \langle (B_p^{\mathrm{min}})^2 \rangle^{1/2})^{1/2}$ versus D, Steenbeck and Krause's choice.

The geostrophic velocity derived from the Taylor's prescription is calculated [equation (11)] and compared to the velocity obtained together with the solution [equation (6)]. Above $D = D_c$, the field has infinitesimal values because induction by the geostrophic velocity is dissipative and the transition is supercritical. Here the weak geostrophic shear, which is $O(B^2)$, cannot identify with the solution ω_1 of (11). A necessary condition for the amplitude of ω_1 to vanish at $D = D_c$ is indeed

$$\int_{-z_1}^{z_1} s B_s \mathbf{B}_p \cdot \mathbf{V} \omega_T dz + \int_{-z_1}^{z_1} \left(B_s \Delta B + B \Delta B_s + \alpha B \frac{\partial B}{\partial z} \right) dz = 0$$

and that amounts to [see (1) and (2)]

$$\lambda \int_{-z_1}^{z_1} B B_s dz = 0,$$

where λ is the eigenvalue at the onset of dynamo action. As D rises above D_c, ω_G increases as $(D - D_c)$ and eventually gets $O(\omega_1)$ amplitude. In the equation for the zonal field B, the term modelling the shearing of the field by the geostrophic velocity is now important and the magnetic field solution seeks to adjust its geometry to obey the Taylor condition. Figure (2) illustrates that mechanism and shows how the geostrophic shear, determined through (6), approaches a "Taylor" limit defined as the solution of (11). From $D \approx -12000$ onwards, the two shears are identical, except, during part of the cycle, for an outer region. Interestingly enough, the ratio of the viscous dissipation (changes in magnetic energy due to shearing of the meridional field by the geostrophic velocity) to the ohmic dissipation, which is zero at the onset of dynamo action, has value of order 1 about the same value of the dynamo number D. That justifies the solution adjusting its geometry to minimize that viscous dissipation, and as a consequence to satisfy the Taylor's constraint. We will deal with these results in a future
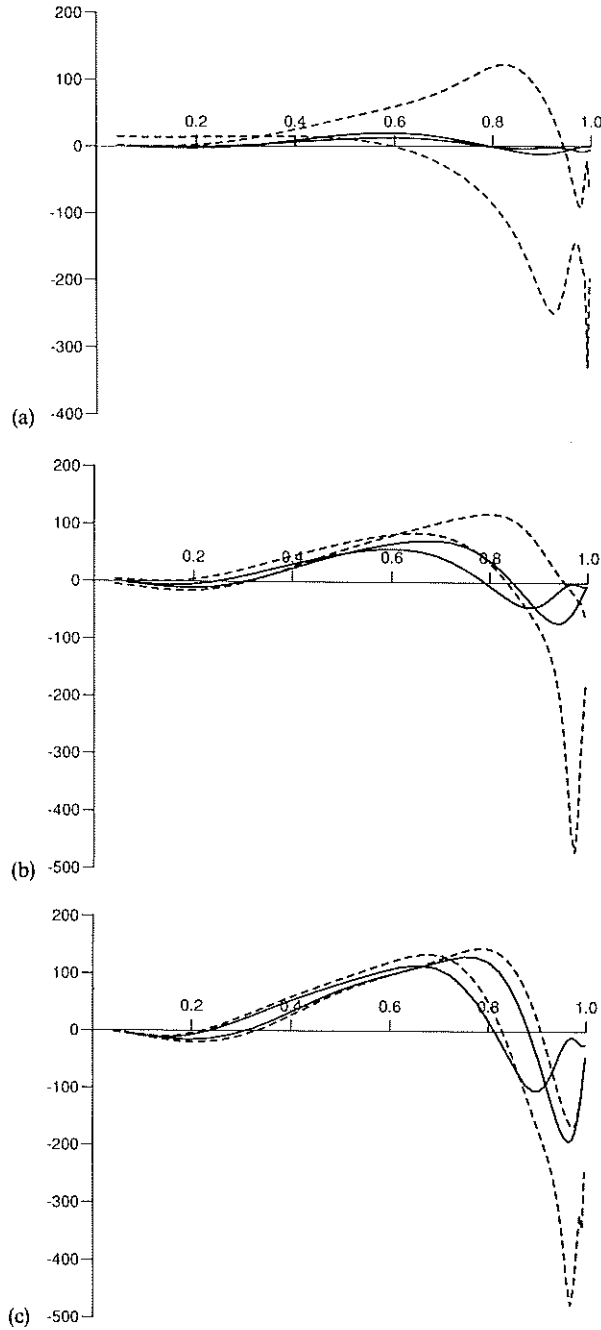
Figure 2   Comparison between $sd\omega_G/ds$ calculated with the time-stepping code (full line) and obtained from (11) (broken line) at two different times of the cycle. (a) $D = -5800$ (b) $D = -7000$ (c) $D = -9000$ (d) $D = -12000$.
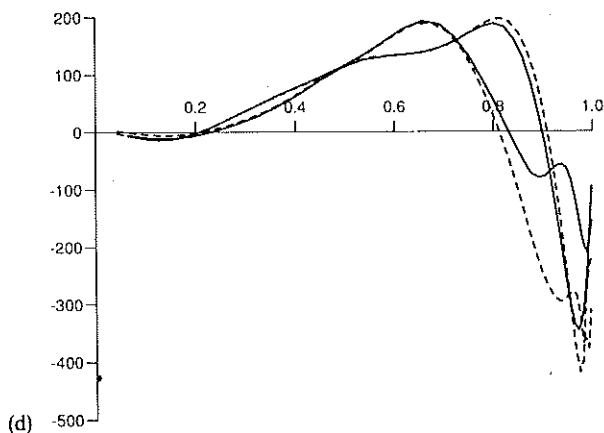
Figure 2 *(Continued)*

paper where we will give evidence of a transition, about $D \approx -12000$, to a branch of mixed parities (dipole and quadrupole) Taylor solutions. Here, let us simply conclude by noting that integrations with a same program have yielded converged solutions for both Braginsky's and Steenbeck and Krause's choices of α and ω effects (see also Anufriyev *et al.*, 1995). Let us now focus on Braginsky's choice.

5. BRAGINSKY'S NUMERICAL MODEL

5.1 *Geometry of the solutions*

The geometry of the solutions is dictated by the forms of both α and ω_T chosen by Braginsky:

$$\omega_T = -3R_\omega s^2(1 - r^2)$$

$$\alpha = 0, \quad s < 0.8$$

$$\alpha = 20R_\alpha\left(\frac{z}{s}\right)\left(1 - \left(\frac{z}{z_1}\right)^6\right)\sin\left[\pi(9 - 10s)\right], \quad s > 0.8.$$

The numerical coefficients entering these expressions and, as a consequence, the dynamo number $D(D = R_\alpha R_\omega)$ are arbitrary. With the convention $D = \max(\alpha)\max(\nabla\omega_T)$, D would be an order of magnitude larger. Most $\alpha\omega$ dynamos are AC and dynamo waves can be expected to travel in the region where both α and ω_T are nonzero. The linear part of the equations (1), (2) is

$$\frac{\partial B}{\partial t} = \Delta B + R_\omega(\mathbf{e}_\phi \times \nabla\omega_T)\cdot\nabla\psi, \tag{12}$$

$$\frac{\partial\psi}{\partial t} = \Delta^-\psi + R_\alpha s\alpha B. \tag{13}$$

With Braginsky's convention, $(\mathbf{e}_\phi \times \nabla \omega_T)$ is directed southwards in the external belts where α is nonzero. As a consequence, the dynamo waves can be expected to propagate northwards in the inner part of the belt, where α is positive and southwards in the outer part (see e.g., Fearn *et al.*, 1988, pp 159–162). If these waves are present in the Braginsky's dynamo model, they are confined to $s > 0.8$, have large wavenumbers and high frequency. The special geometry of α makes another configuration of the magnetic field possible. Out of the equatorial belt $s > 0.8$, the toroidal field B plays no part in the poloidal equation (13). As a first consequence, in most of the volume of the core, the poloidal field ψ obeys a simple diffusion equation; it diffuses from its source, the equatorial belt, to the interior ($s < 0.8$). We expect that there the solution ψ resembles the eigenfunction of the diffusion operator with the smallest decay time (Figure 3). Second, the zonal toroidal field generated in the inner part of the core ($s < 0.8$) from the shearing of the poloidal field ψ by the thermal wind can build up in strength without doing much dynamically. So we expect the toroidal field to be mostly confined to the interior of the core. That large field may anchor the solution and make it steady. In short, a steady-state magnetic field with a poloidal part close to the first eigenfunction of the diffusion operator and with a toroidal part large in the interior of the core but nearly zero in the equatorial belt is a plausible solution of the linear equations (12), (13). This steady state solution is characterized by the separation of the places where respectively the poloidal field and the toroidal field are generated. A numerical integration appears necessary to decide which of the two possible solutions plays the most important role.

5.2 Linear analysis

A linear stability code has been written according to the lines of Barenghi and Jones (1991) (see their appendix). Figure 4 shows the respective growth rates of the two dominant modes. The most easily excited mode is DC. Next, at a second dynamo number, $\alpha\omega$ waves become linearly unstable. The latter mode, when excited, has growth
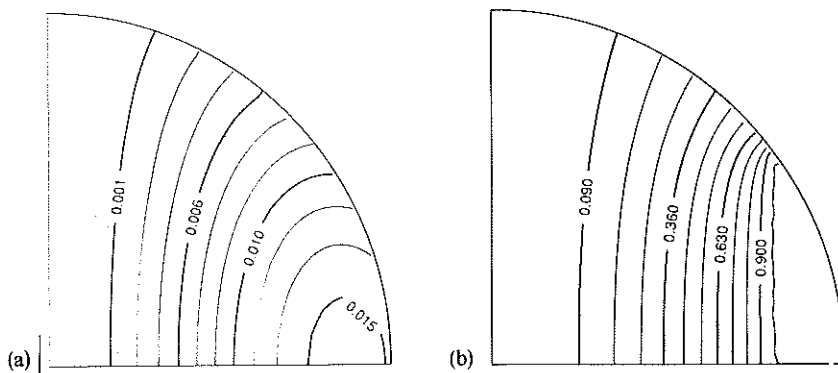

Figure 3 Poloidal diffusive modes $\psi(r, \theta)$ with the largest decay time. (a) For the sphere, (b) For the region $s < 0.8$ with $\psi|_{s=0.8}$ imposed.
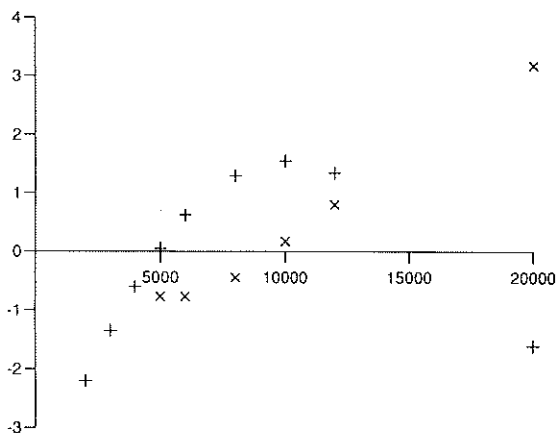
Figure 4   Growth rates λ of the two predominant kinematic mode with respect to the dynamo number D (Braginsky's choice for α and ω). (+) Steady mode with Z-geometry (x) $\alpha\omega$ waves in the outer belt $s \geqslant 0.8$ ($\lambda/100$).

rate O(100) times larger than the former. Unfortunately, it has not been possible to use truncation levels larger than $NL = 28$, $NR = 20$, $NLEG = 8$. So, the initial value code is used to confirm this first study. Table 1 sums up the results which are in agreement with the value $D_c = 5147$ reported by Hofflin and James (1995). It validates the general picture we had from the linear stability code. Table 1 stress how crucial the truncation level of the harmonic expansion at the core surface is. Figure 5 shows the geometry of the eigenmode with eigenvalue 0 at D_c. The toroidal field is nearly zero in the external belt ($r > 0.8$) where the α-effect is nonzero. It implies that a non-linear mechanism is not needed to explain the "flux expulsion" noted by Braginsky. The field at the core surface is nearly dipolar (the ratio between the octupolar and dipolar components is 0.01). The geometry of this mode is indeed everywhere very close to the geometry of the toroidal and poloidal fields with the largest decay time. It explains the Z-like geometry of this kinematic mode (the ratio B_s/B_z is 0.394).

Table 1   Critical dynamo number (onset of dynamo action). Braginsky's dynamo. There are NR points in r and NL points in θ. $NLEG$ Legendre odd degree polynomials are used in the harmonic expansion required to ensure the matching of the field through the boundary with the insulating container

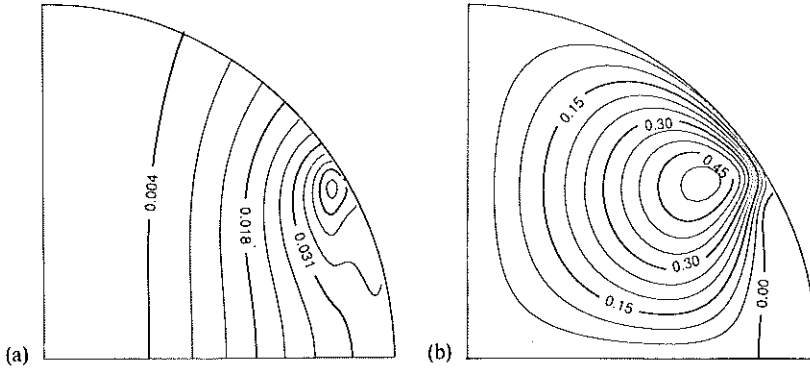| NL	NR	$NLEG$	D_c
40	40	15	5194
50	50	10	6060
50	50	15	5127
50	50	20	5111
60	60	20	5123
60	60	25	5129

Figure 5 The solution at the onset of dynamo action $(D = D_c)$. (a) The field lines of the axisymmetrical meridional field B_p. (b) The contours of equal field strength for the axisymmetrical zonal field B

5.3 The weak-field branch

The investigation of the coupling regime has been cross-checked with the simultaneous study of weak amplitude solutions of numerical model-Z by Hofflin and James (1995). In this regime, the field evolves very slowly towards its equilibrated value. Hence, very long integration times are necessary. It is possible to omit the $\partial \omega_G / \partial t$ term and (6) shall be used. Again, in the limit of small ε, the only important nonlinearity stems from magnetic induction by the geostrophic shear. Since this term is dissipative, the bifurcation structure is supercritical. Above $D = D_c$, at small viscosities, the solution enters the coupling regime and the field scales $\varepsilon^{1/2}$. Figure 6 sums up the evolution of the field amplitude as the dynamo number is increased. This viscously limited solution loses stability at D_T. Table 2 shows that the error on the estimate of the Taylor dynamo number D_T for different truncation levels is quadratic (the numerical schemes are nearly second order accurate); that allows us to estimate $D_T = 11200$ which compares well with $D_T = 10900$ obtained by Hofflin and James (1995). Let us now discuss whether the Taylor's condition plays some part in that regime.

First, a relation such as (11) is no longer available to monitor the approach of this steady solution to the Taylor state. However, we already know that, just above D_c, the evolution of the system can be well described by an amplitude equation for the single kinematic mode m_1, with positive eigenvalue. It can be written as

$$\frac{\partial m_1}{\partial t} = \lambda m_1 - \mu \varepsilon^{-1} m_1^3, \qquad (14)$$

where $\lambda(D)$ is the linear growth rate, the term $-\mu(D)\varepsilon^{-1}m_1^3$ is induction by the geostrophic velocity ω_G; μ is positive. Indeed, just above D_c, the field amplitude increases with D as $\sqrt{D - D_c}$. Furthermore, Figure 4 (or rather, with a better resolution, Figure 1 of Hofflin and James, 1995), showing the evolution of λ with D, is very similar to Figure 6 showing the evolution of the amplitude of the field in the Ekman regime. This is the first indication of the relation (14), with μ nearly constant, describing
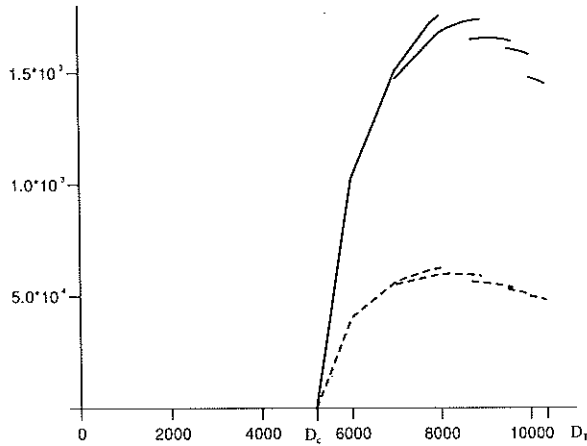
Figure 6   Average amplitude of the field on the Ekman branch versus $(D/100)$. Continuous line: $\langle B^2 \rangle^{1/2}$, broken curve: $\langle B_z^2 \rangle^{1/2}$. As D is increased larger grid sizes are required. Results from integrations with $N = 40$, $N = 50$, $N = 60$, $N = 70$, $N = 80$ are plotted $\varepsilon = 10^{-5}$.

Table 2   Taylor dynamo number. Braginsky's dynamo

NL	NR	$NLEG$	D_T
40	40	15	8100
50	50	20	9000
60	60	25	9700
70	70	30	10200
80	80	35	10350

the evolution of the field throughout the steady Ekman regime. That is further confirmed by Figure 7 which shows that, for $D = 10000$, the non-linear solution has a geometry identical to the kinematic mode. It means that, contrary to what has been described above for the "Steenbeck and Krause" choice for α and ω, there is no progressive adaptation to the Taylor's condition, throughout most of the Ekman regime, and viscous dissipation is here negligible compared to ohmic dissipation (in the ratio 10^{-4} to 1). Now, the stability of the non-linear solution satisfying (14) reduces to the original linear stability problem where ω_T would now stand for $\omega_G + \omega_T$. The growth rate of m_1 for this new linear problem is exactly 0 but there should be a dynamo number above which a second mode has positive growth rate. It turns out that the Ekman branch solution loses stability at a dynamo number very close to the dynamo number for which the second kinematic mode (dynamo waves propagating in the outer belt, see the linear analysis) has positive growth rate ($D = 11660$ after Hofflin and James, 1995). This second mode has to be called for to describe how the solution settles to equilibrium, just below D_T. There is a narrow range of dynamo numbers D, for which both modes take part in the equilibrated solution. Just below, the dynamo waves play
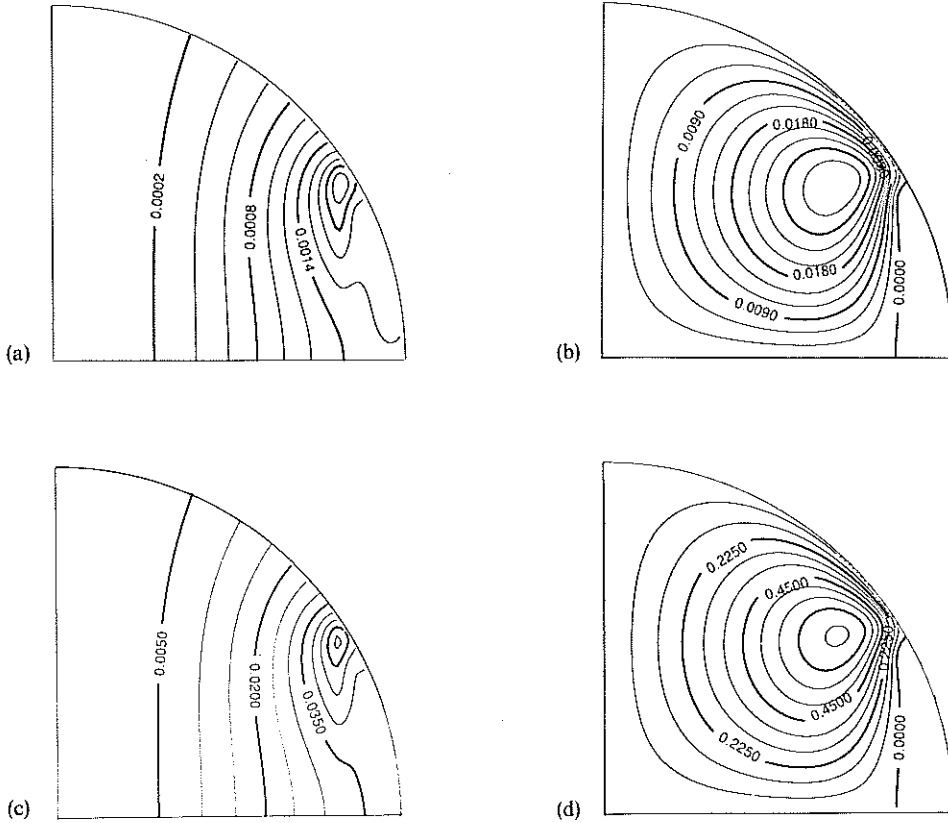
Figure 7 Comparison between the geometry of the solution on the Ekman branch (a) and (c) and the geometry of the kinematic model (b) and (d). $D = 10000$, (a) and (c) meridional field, (b) and (d) zonal field.

a part in the transient solution but are eventually damped. This scenario is similar to what has been described for some $\alpha^2\omega$ dynamos (Barenghi, 1993): steady Ekman state followed by vacillating Ekman and steady Taylor states.

Above $D = 15000$, the kinematic steady mode is linearly stable. The null solution is however unstable. Indeed, the complex conjugate pair of eigenvalues of the kinematic modes made of $\alpha\omega$ waves propagating in the external belt keeps positive real part. That growth rate is very large $Re(\lambda) = O(100)$ and starting from an initial random infinitesimal field, the waves grow quickly until their amplitude reaches an equilibrium value which scales as $\varepsilon^{1/2}$. This solution is transient because the geostrophic velocity associated with the $\alpha\omega$ waves adds to the thermal wind to make the steady mode unstable. The field strength increases until it is $O(1)$. The final solution is steady. In the range $11000 < D < 15000$, both modes are linearly unstable and the dynamo waves play a part in the transient evolution of the field because their growth rate $Re(\lambda) = O(100)$ is large compared with the growth rate of the steady mode $\lambda = O(1)$.

5.4   *The strong-field branch*

At D_T, the amplitude of the transient field exponentially increases until it becomes O(1). Here, the $\partial \omega_G / \partial t$ term is required to prevent numerical instabilities whilst converging to the final steady solution. The final solution is inviscid and does not change any further as the viscosity is decreased below 3×10^{-5}. Its geometry (Figure 8) is quite close to what is found in the coupling regime. That had already been reported for α^2 dynamo models (Barenghi, 1992). Figure 9 shows how the amplitude of the field changes with the dynamo number D (for $\varepsilon = 10^{-5}$). Solutions exist for $D \geqslant 1300$, well below $D_c = 5100$. Figure 10 shows the geometry of this subcritical solution ($D = 1300$) and Table 4 illustrates its inviscid character. With larger ε, viscous dissipation cannot
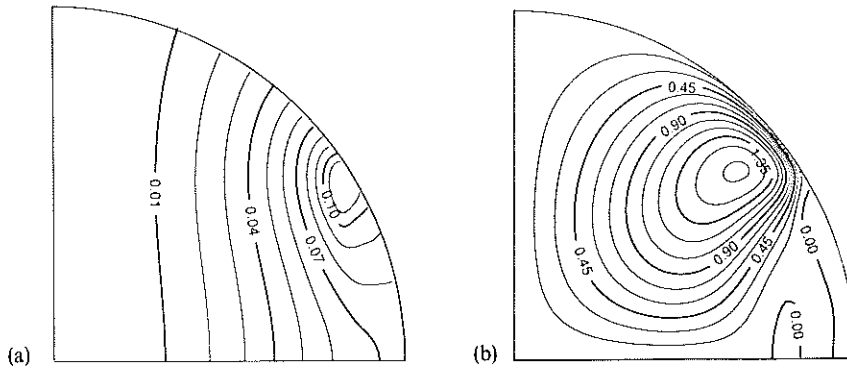

Figure 8   The inviscid solution. $D = 10200$. (a) The field lines of the axisymmetrical meridional field B_p. (b) The contours of equal field strength for the axisymmetrical zonal field B.
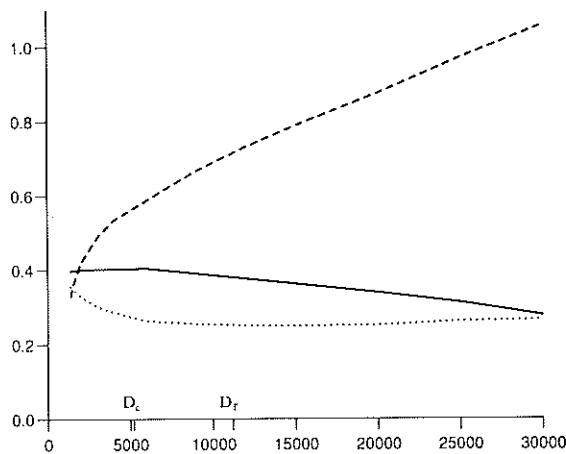

Figure 9   Amplitude of the solution versus D. $\varepsilon = 10^{-5}$. Continuous curve: B_s/B_z. Dotted line: B_z. Broken line: zonal field B, $NL = 180$ $NR = 120$.
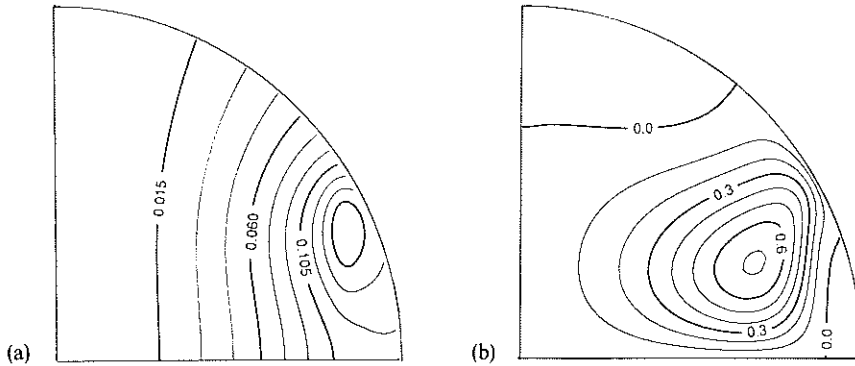
Figure 10 The solution at the highly subcritical dynamo number $D = -1300$. (a) The field lines of the axisymmetrical meridional field B_p. (b) The contours of equal field strength for the axisymmetrical zonal field **B**.

Table 3 Amplitude of the inviscid solution. $D = 10200$, $NR = NL = 70$, $NLEGE = 30$

ε	$\langle B_z \rangle$	$\langle B \rangle$	$\langle B_s \rangle / \langle B_z \rangle$
10^{-4}	0.2661	0.749	0.362
3×10^{-5}	0.2552	0.729	0.376
10^{-5}	0.2517	0.721	0.383
10^{-6}	0.2500	0.717	0.388

Table 4 Same as Table 3. $D = 1300$, $NR = NL = 60$, $NLEGE = 20$

ε	$\langle B_z \rangle$	$\langle B \rangle$	$\langle B_s \rangle / \langle B_z \rangle$
10^{-3}		$\varnothing$	
3×10^{-4}	0.312	0.262	0.390
10^{-4}	0.333	0.294	0.393
3×10^{-5}	0.338	0.300	0.396
10^{-5}	0.339	0.301	0.396

be neglected and larger dynamo numbers are required to get finite amplitude solutions. Above $D \approx 3000$, the geometry of the solution changes very little. The ratio B_s/B_z decreases with D, as Roberts (1989) found. Finally, we have compared out results with the findings of Braginsky (1978) and Braginsky and Roberts (1987) which had been obtained for $D = 25000$ and much larger viscosities.

First, their results for $\varepsilon = 0.01$ are duplicated. Then, the evolution of the solution from $\varepsilon = 0.01$ to the limit of vanishing viscosities is monitored (Figure 11). From $\varepsilon = 0.01$ to $\varepsilon = 0.001$, the ratio B_s/B_z decreases and, as a consequence, the solution for $\varepsilon = 0.001$ is strikingly axial (Figure 12a,b). However, from $\varepsilon = 0.001$ downwards, the ratio B_s/B_z increases again. Thus, the Taylor condition is not met by aligning the lines
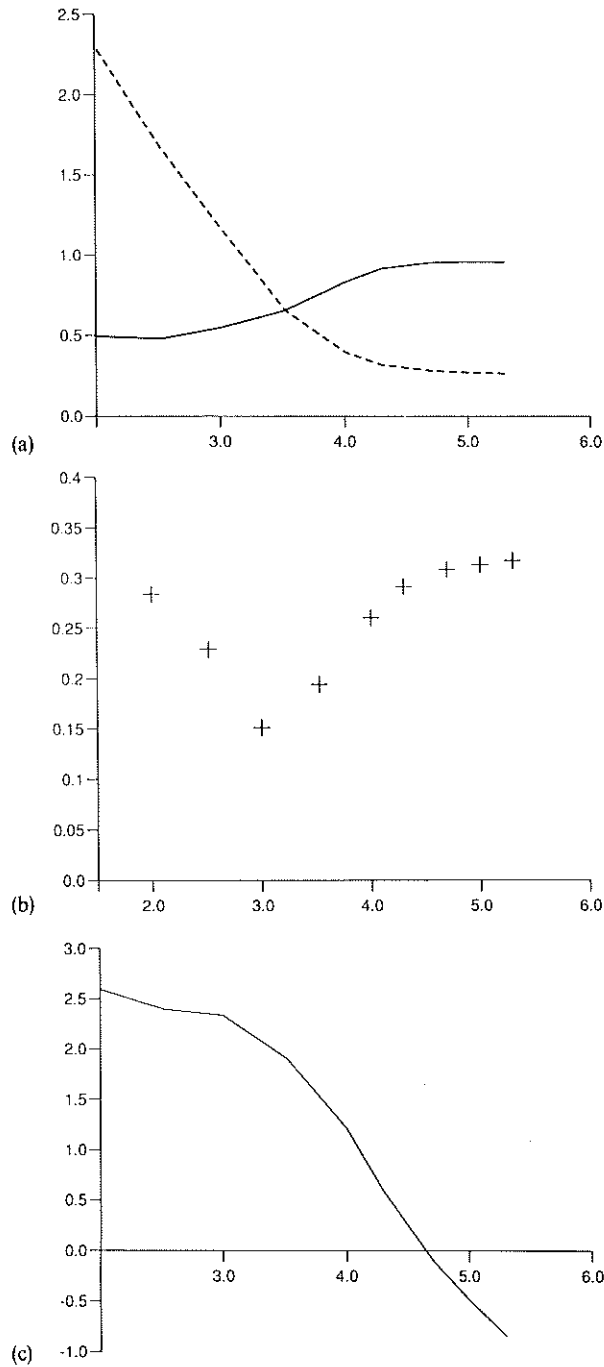
Figure 11 Amplitude of the solution versus $-\log_{10}\varepsilon^{-1}$, $D = 25000$. (a) Full line: zonal field strength $\langle B^2 \rangle^{1/2}$ broken line: meridional field strenth $\langle B_p^2 \rangle^{1/2}$. (b) $\langle B_s^2 \rangle^{1/2}/\langle B_z^2 \rangle^{1/2}$. (c) $\log_{10}(Q_v)$ where Q_v is viscous dissipation during one unit time. (d) $(+)\, Q_v(\times)Q_J$, where Q_J is ohmic dissipation ($NL = NR = 120$).
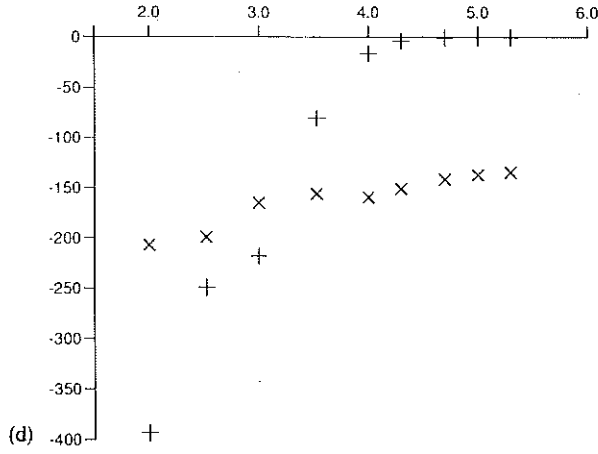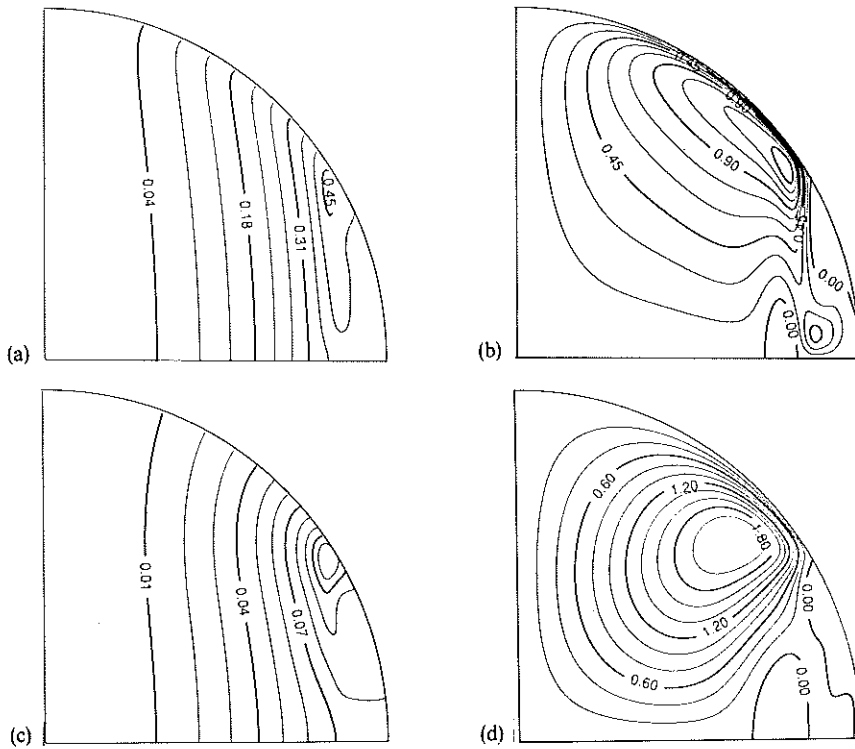
Figure 11   *(Continued).*

Figure 12   The evolution of the geometry of the solution ($D = 25000$) from $\varepsilon = 10^{-3}$ (a) and (b) to $\varepsilon = 5.10^{-6}$ (c) and (d). (a) and (c) The field lines of the axisymmetrical meridional field B_p. (b) and (d) The contours of equal field strength for the axisymmetrical zonal field $B(NL = NR = 120)$.

of force of the poloidal field parallel to the symmetry axis, and for intermediate values of the viscosity, the geostrophic velocity (Figure 13a) does not grow as ε^{-1} mainly because the intensity of the poloidal field decreases sharply. As ε is further decreased, the magnetic field solution (Figure 12c,d) and the geostrophic shear $\omega_G(s)$ (Figure 13b) also tend towards an inviscid limit. The geometry of this inviscid solution is smooth, as indicated also by the small ohmic dissipation. Figure 13b shows evidence of a singularity at the symmetry axis. Its discussion is delayed until the next section. The collapse of the viscous dissipation (calculated as the change in magnetic energy due to the term $sB_s d\omega_G/ds$) is perhaps the most striking consequence of the approach to the Taylor
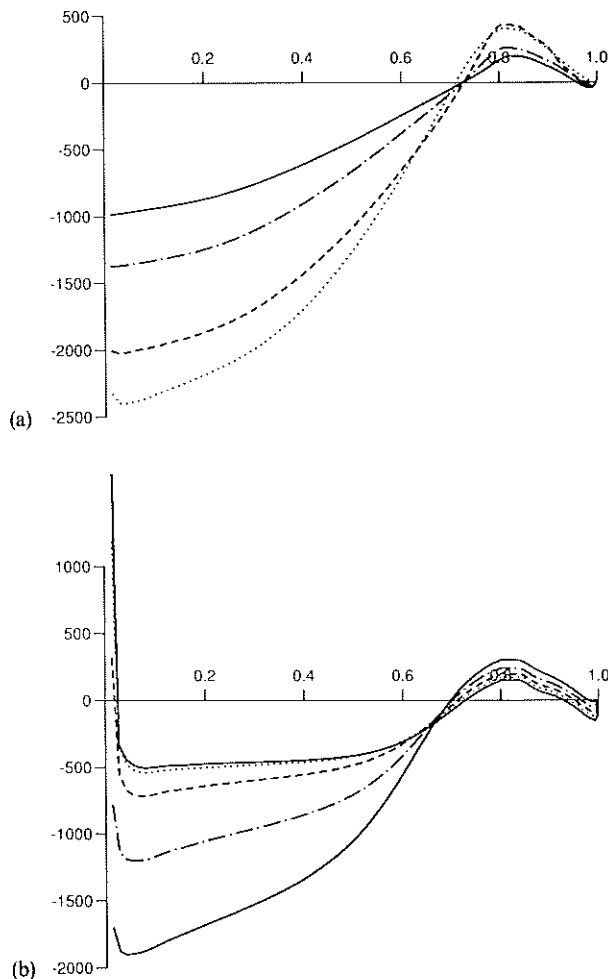

Figure 13 The geostrophic shear $\omega_G(s)$ as a function of the distance from the polar axis, $D = 25000$ $(NL = NR = 120)$. (a) Full line $\varepsilon = 10^{-2}$, half dotted half broken line $\varepsilon = 3 \times 10^{-3}$, broken line $\varepsilon = 10^{-3}$, dotted line $\varepsilon = 3 \times 10^{-4}$. (b) Full line $\varepsilon = 10^{-4}$, half-dotted half-broken line, $\varepsilon = 5 \times 10^{-5}$ broken line $\varepsilon = 2 \times 10^{-5}$, dotted line $\varepsilon = 10^{-5}$, full line $\varepsilon = 5 \times 10^{-6}$.

Table 5   Braginsky's asymptotics. R_ω scales as $\varepsilon^{-1/3}$

D	R_ω	R_α	ε	$\langle B_z \rangle$	$\langle B_s \rangle / \langle B_z \rangle$
4641	146.8	31.62	10^{-3}	0.360	0.383
6934	219.3	31.62	3×10^{-4}	0.301	0.369
10000	316.2	31.62	10^{-4}	0.272	0.364
14938	472.4	31.62	3×10^{-5}	0.250	0.350
21544	681.2	31.62	10^{-5}	0.245	0.320
25000	500	50	10^{-2}	2.23	0.281
33930	676.8	50	4×10^{-3}	1.48	0.264

regime (Figure 11c). Once the Taylor limit is attained, viscous dissipation scales rightly as ε. Now, the asymptotic form ($\varepsilon \to 0$) proposed by Braginsky (1975) was

$$\omega_G = O(\varepsilon^{-2/3}), \quad B_s = O(\varepsilon^{1/3}), \quad B_T = O(1), \tag{15}$$

with

$$R_\alpha = O(1), \quad R_\omega = O(\varepsilon^{-1/3}).$$

Since R_ω changes as $\varepsilon^{-1/3}$, there is no straightforward contradiction with the finding of inviscid regimes. Braginsky and Roberts (1987) noticed that their numerical results, limited to large values of the viscosity $\varepsilon = 0.004 - 0.04$, do not rule out (15). Table 5 sums up the results, obtained with smaller D, together with those duplicating Braginsky and Roberts results. The asymptotic form (15) is not vindicated.

In a recent paper, Braginsky and Roberts reinvestigate the strong field branch of the Braginsky's model. They pay particular heed to the quantities Q_v, Q_J, respectively the viscous and ohmic dissipation. They oppose "Taylor-like" ($Q_v \ll Q_J$) to "Model-Z-like" ($Q_v \approx Q_J$) solutions. A detailed comparison with the present paper is not possible because they study $\varepsilon > 2 \times 10^{-3}$ whereas we mainly investigate the approach to the inviscid limit. Their results indicate also an evolution from "Model-Z-like" to "Taylor-like" solutions as ε is decreased. Figure 11d (with $D = 25000$) is added to allow further comparison with the Braginsky and Roberts (1994) study.

6. DISCUSSION

Reinstating the $\partial \omega_G / \partial t$ term in the equation for the geostrophic shear (7) has allowed us to reach the inviscid limit of the Braginsky's numerical model. Each of the solutions obtained with (7) has been checked against the $Ro/\varepsilon \to 0$ limit. Once a converged steady solution is obtained, it can be used as a starting point for a numerical integration without the inertial term, provided the time-steps are small enough. The solutions obtained respectively in the limit $Ro/\varepsilon \to 0$ and with $Ro = 0$ are identical. It demonstrates that the new ingredient plays here a mere technical role, helping to prevent numerical instabilities. Let us consider a numerical

error e on the term

$$\frac{d}{ds}\left(s^2 \int_{-z_1}^{z_1} B_s B\, dz \right).$$

The ensuing error on ω_G is $\varepsilon^{-1} e$ as the inertial term is omitted whereas it is only $Ro^{-1} dt\, e$ as it is reinstated (the typical time step dt is 5×10^{-6} and $Ro^{-1} dt$ is typically on the order of 10). Thus, the inertial term $\partial \omega_G / \partial t$ attenuates the stiffness inherent in the calculation of the geostrophic velocity with (6) and turns out to be an efficient way to study inviscid branches.

In Section 5.4, we have used (7) only as a way to approach (6). However, another limit of the equation (7) is worth pointing out. Setting $\varepsilon = 0$ in (7), we get an equation for torsional oscillations

$$Ro\frac{\partial \omega_G}{\partial t} - \frac{1}{z_1 s^3}\frac{d}{ds}\left(s^2 \int_{-z_1}^{z_1} B B_s\, dz \right) = 0 \tag{16}$$

which can also be used along with (1) and (2) to time-step the evolution of the field. Indeed, the inviscid branch of the Braginsky's model can also be attained this way (from e.g. an initial random field). These solutions are close to the solutions discussed in Section 5.4 ($\varepsilon \neq 0, \varepsilon \rightarrow 0$). There are however differences (see Figure 14), which have to be explained. From (6) and (16), we can derive two different integral conditions on the geostrophic velocity. Equation 6 yields

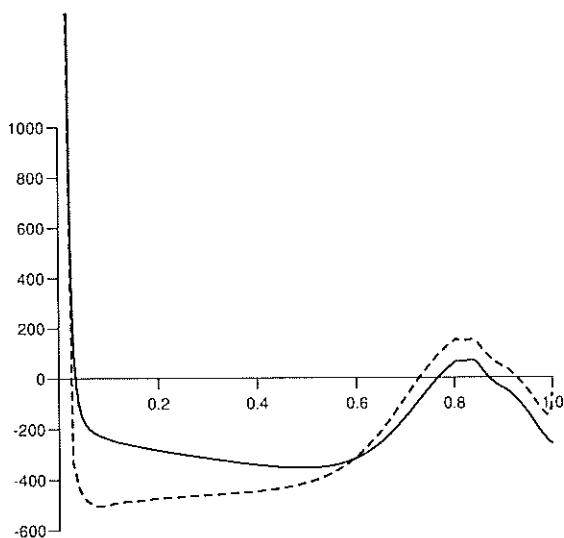$$\int_0^1 \frac{s^3 \omega_G(s)}{z_1^{1/2}}\, ds = 0 \tag{17}$$

Figure 14 Same as Figure 13. Full line $\varepsilon = 0$, broken line $\varepsilon = 10^{-5}$. $NL = 180$, $NR = 120$.

[and $\omega_G(1) = 0$] whatever the viscosity is. This identity states that the net viscous torque acting on the mantle is zero (because no other torque balances it). Asymptotic solutions ($\varepsilon \to 0$) calculated with (6) have to satisfy (17) on top of the Taylor's condition. On the other hand, we get from (16)

$$\int_0^1 s^3 z_1 \frac{\partial \omega_G}{\partial t}(s) \, ds = 0. \tag{18}$$

This states that there is conservation of the core angular momentum and still holds in the limit $Ro \to 0$. The integral conditions (17), (18) are a first indication that both limits ($\varepsilon \to 0$), and $Ro \to 0$ are singular. The additional constraint $\omega_G(1) = 0$ makes however condition (17) more stringent since it is not possible to add simply a bulk rotation to the solution to make ω_G satisfy (17). It can be checked that all the geostrophic velocity solutions obtained with (6) obey the condition (17). To this end, the ratio

$$R = \left[\int_0^1 z_1^{-1/2} s^3 |\omega_G| \, ds \right]^{-1} \int_0^1 z_1^{-1/2} s^3 \omega_G \, ds.$$

is calculated, imposing $\omega_G(1) = 0$. R is zero when (17) is satisfied. All the solutions, for the numerical model of Braginsky, calculated with either (6) or (7) (with $R_0 \ll \varepsilon$) yield $R \leqslant 0.10$. In contrast, the geostrophic velocity solution shown on Figure 15 yields $R = 0.89$. Now, the constraint $\omega_G(1) = 0$. arises because, using (6) or (7), we don't model the vertical boundary layer that replace the Ekman layer at the equator. So the difference between the solutions respectively for $\varepsilon = 0$ and $\varepsilon \ll 1$ points to a limitation of the model. Let us now discuss another interesting feature of the limits ($\varepsilon \to 0$) and $Ro \to 0$.

With $\varepsilon = Ro = 0$., the geostrophic velocity doesn't play a role as such. Indeed, in this Taylor regime, ω_G is determined only through its role in the induction equation, where $s d\omega_G/ds$ alone plays a part. Hence, ω_G loses here some of its physical meaning. In particular, an inspection of the induction equation shows that $s d\omega_G/ds$ can be O(1) at the axis (see also Section 2). In that event, $\omega_G \to \infty$ logarithmically as $s \to 0$. Let us illustrate further this point. In the neighbourhood of the axis, the magnetic field and velocity components can be expanded as:

$$B = b_0(z)s + b_1(z)s^3 + O(s^5), \quad \psi = \psi_0(z)s^2 + O(s^4), \quad \chi = \chi_0(z)s^2 + O(s^4).$$

Then, the induction equation for the zonal field B at the order 1 in s is:

$$\frac{\partial b_0}{\partial t} = \left(9b_1 + \frac{\partial^2 b_0}{\partial z^2} \right) - \left(s \frac{\partial \omega_G}{\partial s} \right) \frac{\partial \psi_0}{\partial z} + \left(b_0 \frac{\partial \chi_0}{\partial z} - 2 \frac{\partial}{\partial z}(b_0 \chi_0) \right)$$

where, to simplify the discussion, $\omega_T = O(s^2)$ is assumed (such is the case for the Braginsky's model). The zonal field vanishes at the boundary with the mantle ($b_0(1) = b_1(1) = 0$). So, we find that in the Taylor regime ($\chi_0(1) = 0$):

$$s \frac{\partial \omega_G}{\partial s} = \frac{\partial^2 b_0}{\partial z} \bigg|_{z=1-} \bigg/ \frac{\partial \psi_0}{\partial z} \bigg|_{z=1-} \neq 0.$$

Because this singularity is intolerable from a physical standpoint, such a solution cannot be found while using equations such as (7) and (8) where the quantity ω_G bears a physical meaning. This was discussed by Proctor (1975) and Fearn and Proctor (1987), who suggested that in the presence of viscosity it would be accommodated by a passive boundary layer. So, when we speak of "Taylor states" (Section 5.4), we mean that core-mantle coupling plays no essential role over the surface ($r = 1$) except near the symmetry axis $s = 0$. Surrounding the axis is a region where viscosity is important, and in which the logarithmic singularity in ω_G is removed so that $\omega_G(0)$ is finite as is demanded on physical grounds. Investigation of that boundary layer deserves further work; it has not been possible to resolve its structure with the code used in the present study.

Hopefully, the study of nearly axisymmetrical dynamo models will help us to decide how to calculate the geostrophic velocity in dynamic geodynamo models. Here, it has allowed us to suggest a new method to attain the inviscid limit and to discuss the nature of that limit. Now, another ingredient, magnetic coupling with the mantle (and with the inner core as well), should be added to model more closely the Earth's outer core. It has been cautiously argued (e.g. Roberts, 1989) that magnetic coupling can be simulated, with qualitative correctness, by increasing the strength of the viscous coupling. As a matter of fact, it is not clear whether one of the two core-mantle couplings, viscous or magnetic, is predominant. Present estimates of the conductivity of the lower mantle are lower than 10 years ago (around $10\,\mathrm{Sm}^{-1}$) (Peyronneau and Poirier, 1989; Li and Jeanloz, 1989; Shankland *et al.*, 1993) and the conductance of the mantle (the integral of the electrical conductivity over depth) may be no larger than 10^7 S. Such an estimate makes the strength of the two couplings comparable. Furthermore, at low amplitudes, it is erroneous to mimic magnetic coupling by viscous coupling. Braginsky (1975) has shown that when a thin conducting layer is added at the bottom of the mantle, the boundary condition for the poloidal field is not changed at the first order and that the boundary condition for the zonal toroidal field can be written:

$$B = -\mu\Sigma\left(\frac{1}{\mu\sigma}\frac{\partial B}{\partial r} + v_\phi B_r\right)$$

where Σ is the conductance of the conducting layer. The Taylor condition, with nonzero toroidal zonal field at the CMB, yields:

$$\forall s \qquad \frac{1}{s^2}\frac{d}{ds}\left(s^2\int_0^{z_1} BB_s dz\right) = -\frac{a}{z_1}(BB_r)(s, z_1).$$

Taking into account the nonzero magnetic wind at the core surface, we get, in dimensionless form:

$$\frac{\Sigma}{a\sigma}\left\{\left[\omega_G(s) + \left(\frac{B(s, z_1)}{s}\right)^2\right]B_r^2(s, z_1) + \frac{1}{s}\frac{\partial B}{\partial r}\bigg|_{r=1_-} B_r(s, z_1)\right\} = \frac{z_1}{s^3}\frac{d}{ds}\left(s^2\int_0^{z_1} BB_s dz\right). \quad (19)$$

With infinitesimal magnetic field, ω_G given by (19) is independent of the amplitude of the field and is nonzero. Here, the weak field branch may not exist altogether. So, at low

magnetic field amplitude, magnetic and viscous coupling play very different roles (see also Fearn and Proctor, 1992). Combining (6) and (19), we get a more general equation for the geostrophic velocity, with two small parameters ε and $\Sigma/a\sigma$. With $\varepsilon \neq 0$, it is readily checked that even if $\varepsilon \ll \Sigma/a\sigma$, the bifurcation structure, at the onset of dynamo action, is still supercritical. And as D is increased above D_c, the solution scales as $\varepsilon^{1/2}$, and not as $(\Sigma/a\sigma)^{1/2}$. The large amplitude case requires also additional studies. Braginsky (1988) and Cupal and Hejda (1989) have shown that finite amplitude solutions relying either on viscous coupling or on magnetic coupling are qualitatively similar. However, these studies have attained neither the inviscid limit nor the small conductance limit.

The steadiness, dipolar geometry, and O(1) amplitude of the Braginsky's numerical model are the characteristics that make it a reference model. In particular, it illustrates that predominance of magnetic diffusion in a large part of the core is one possible explanation for the mainly dipolar geometry of the Earth's magnetic field. That is reminiscent of a recent study by Hollerbach and Jones (1993) who stressed the role played by the region inside the cylinder tangent to the inner core to make the dynamo steadier and to favour the dipole component of the field.

Acknowledgements

References

Anufriyev, A. P., Cupal, I. and Hejda, P., "The Taylor state in $\alpha\omega$ dynamos," *Geophys. Astrophys. Fluid Dynam.* submitted (1995).

Barenghi, C. F., "Nonlinear planetary dynamos in a rotating spherical shell II. The post Taylor equilibration for α^2 dynamos," *Geophys. Astrophys. Fluid Dynam.* **67**, 27–36 (1992).

Barenghi, C. F., "Nonlinear planetary dynamos in a rotating spherical shell III. $\alpha^2\omega$ models and the geodynamo," *Geophys. Astrophys. Fluid Dynam.* **71**, 163–185 (1992).

Barenghi, C. F. and Jones, C. A., "Nonlinear planetary dynamos in a rotating spherical shell I. Numerical methods," *Geophys. Astrophys. Fluid Dynam.* **60**, 211–243 (1991).

Braginsky, S. I., "Self excitation of a magnetic fluid during the motion of a highly conducting fluid," *Soviet Phys. JETP* **20**, 726–735 (1964).

Braginsky, S. I., "Nearly axially symmetric model of the hydromagnetic dynamo of the Earth I," *Geomagn. Aeron.* **15**, 122–128 (1975).

Braginsky, S. I., "Nearly axially symmetric model of the hydromagnetic dynamo of the Earth," *Geomagn. Aeron.* **18**, 225–231 (1978).

Braginsky, S. I., "The Z model of the geodynamo with magnetic friction," *Geomagn. Aeron.* **28**, 407–412 (1988).

Braginsky, S. I. and Roberts, P. H., "A model-Z Geodynamo," *Geophys. Astrophys. Fluid Dynam.* **38**, 327–349 (1987).

Braginsky, S. I. and Roberts, P. H., "From Taylor-state to Model-Z," *Geophys. Astrophys. Fluid Dynam.* **77**, 3–13 (1994).

Cupal, I. and Hejda, P., "On the computation of a model-Z with electromagnetic core-mantle coupling," *Geophys. Astrophys. Fluid Dynam.* **49**, 161–172 (1989).

Fearn, D. R. and Proctor, M. R. E., "Dynamically consistent magnetic fields produced by differential rotation," *J. Fluid Mech.* **178**, 521–534 (1987).

Fearn, D. R. and Proctor, M. R. E., "Magnetostrophic balance in non-axisymmetric non-standard dynamo models," *Geophys. Astrophys. Fluid Dynam.* **67**, 117–128 (1992).

Fearn, D. R., Roberts, P. H. and Soward, A. M., "Convection, stability and the dynamo," in: *Energy Stability and Convection* (Eds. G. P. Galdi and B. Straughan) Pitman Research notes in Mathematics series **168** Longman, 60–324 (1988).

Hofflin, P. W. and James, R. W., "Small amplitude solutions of model-Z," *Geophys. Astrophys. Fluid Dynam.* in preparation (1995).

Hollerbach, R. and Ierley, G. R., "A modal α^2-dynamo in the limit of asymptotically small viscosity," *Geophys. Astrophys. Fluid Dynam.* **56**, 133–158 (1991).

Hollerbach, R. and Jones, C. A., "Influence of the Earth's inner core on geomagnetic fluctuations and reversals," *Nature*, **365**, 541–543 (1993).

Hollerbach, R., Barenghi, C. F. and Jones, C. A., "Taylor's constraint in a spherical $\alpha\omega$-dynamo," *Geophys. Astrophys. Fluid Dynam.* **67**, 3–25 (1992).

Li, X. and Jeanloz, R., "Measurement of the electrical conductivity of a perovskite-magnetowüstite assemblage," *EOS* **70**, 1369 (1989).

Malkus, W. V. R. and Proctor, M. R. E., "The macrodynamics of α-effect dynamos in rotating fluids," *J. Fluid Mech.* **67**, 417–443 (1975).

Peyronneau, J. and Poirier, J. P., "Electrical conductivity of the Earth's lower mantle," *Nature* **342**, 537–539 (1989).

Poirier, J. P., "Transport properties of liquid metals and viscosity of the Earth's core," *Geophys. J.* **92**, 99–105 (1988).

Proctor, M. R. E., "Nonlinear mean field dynamo models and related topics," PhD Thesis, University of Cambridge (1975).

Roberts, P. H., "Kinematic dynamo models," *Phil. Trans. R. Soc. Lond.* A **272**, 663–698 (1972).

Roberts, P. H., "From Taylor-state to model-Z," *Geophys. Astrophys. Fluid Dynam.* **49**, 143–160 (1989).

Shankland, T. J., Peyronneau, J. and Poirier, J. P., "Electrical conductivity of the Earth's lower mantle," *Nature* **366**, 453–455 (1993).

Taylor, J. B., "The magneto-hydrodynamics of a rotating fluid and the earth's dynamo problem," *Proc. R. Soc. Lond.* A **274**, 274–283 (1963).

Tough, J. G. and Roberts, P. H., "Nearly symmetric hydromagnetic dynamos," *Phys. Earth planet. Inter.* **1**, 288–296 (1968).